

Eliminating Blind Spots for Assisted Driving

Tobias Ehlgen, Tomáš Pajdla, and Dieter Ammon

Abstract—Drivers of heavy goods vehicles are not able to survey the whole surrounding area of their vehicle due to large blind spot regions. This paper shows how catadioptric cameras—a combination of cameras and mirrors—can be used to survey the surrounding area of vehicles. Four such cameras were mounted on a truck–trailer combination, and the images are combined such that obstacles are visible in an image presented to the driver. This image is a bird’s eye view of the vehicle. Additionally, corridors indicating the path of motion of the vehicle are overlaid to the resulting image. To compute those corridors, a mathematical description of the path of motion is derived. Such a system does not only support the driver during maneuvering tasks but also increases safety of driving large vehicles.

Index Terms—Automotive vision, catadioptric cameras, omnidirectional vision, panoramic vision, single-track model.

I. INTRODUCTION

MANY PEOPLE lose their lives in accidents involving trucks every year [1]. Most of the fatal accidents happen due to the limited sight of truck drivers. To cope with this problem, some countries implement legal requirements that enforce using either cameras or mirrors to provide drivers with a complete view of the vehicle surrounding area. The main disadvantage of mirrors is that areas around the truck are differently magnified. Therefore, objects near the truck only cover small parts of the mirror surface and hence are not clearly visible, particularly, when the driver turns right and needs to check up to six mirrors at the same time.

The largest blind spot areas emerge behind and on the right-hand side of the vehicle because the driver sits on the left-hand side (Fig. 1). Large blind spot areas are also in front of the vehicle. These areas are not visible from the driver’s position due to the shape of the truck.

This paper shows how catadioptric cameras—a combination of mirrors and standard cameras—are used to provide drivers with an image allowing to survey the whole surrounding area of their vehicle, including truck and trailer. The introduced approach combines four catadioptric cameras in such a way that a bird’s eye view image—a view of the whole surrounding area of the vehicle from above—is shown to the driver.

To generate a true bird’s eye view image, the angle between the truck and the trailer, referred to as *kink angle*, must be

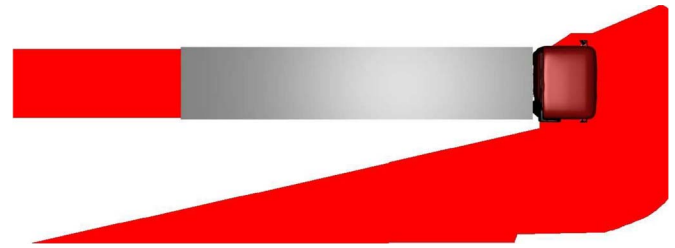


Fig. 1. Blind spot region (red) of the truck–trailer combination shown on the ground plane. The width of the vehicle is about 2 m. A large blind spot region arises in front of the vehicle as well as on the passenger’s side.

determined while driving. This is accomplished here by using a single-track model of the vehicle. To show the accuracy of this model, the kink angle determined by the single-track model is compared to the kink angle given by a sensor mounted at the joint connecting truck and trailer. However, such a sensor cannot be installed into series-production vehicles due to automotive requirements and costs.

Since the motion of an articulated vehicle is complex, a simulated corridor is overlaid onto the resulting image to indicate the trajectory of the vehicle and to assist the driver while maneuvering. This paper is organized as follows. First, previous work is reviewed in Section II. Section III introduces the bird’s eye view system. This system consists of four catadioptric cameras mounted on a truck and trailer. The images are rectified and combined. Additionally, a corridor is overlaid onto the bird’s eye view image showing the trajectory of the vehicle. Finally, the system is evaluated in Section IV.

II. PREVIOUS AND RELATED WORK

Recently, interesting and useful catadioptric cameras, i.e., those that combine lenses and mirrors, have been designed (Fig. 2).

These cameras capture a large field of view in a single image. Among such catadioptric systems, perhaps the most interesting ones are those with a single effective viewpoint [2]. The advantages of single viewpoint catadioptric systems are that traditional and well-known computer vision geometry can be applied, and the images can correctly be transformed to perspective images.

It is known [2] that only six catadioptric systems preserve the single viewpoint constraint, which are planar, conical, spherical, ellipsoidal, paraboloidal, and hyperboloidal mirrors. Hyperboloidal mirrors are the only mirrors among those that in combination with a pinhole camera enlarge the field of view and preserve the single viewpoint constraint. Since standard pinhole cameras meet the demands of automotive vision systems, hyperboloidal mirrors in combination with pinhole cameras are used in the bird’s eye view system.

Manuscript received January 17, 2008; revised July 13, 2008 and August 27, 2008. First published November 17, 2008; current version published December 1, 2008. The work of T. Pajdla was supported by the MSM6840770038 DMCMIII Grant. The Associate Editor for this paper was C. Stiller.

T. Ehlgen and T. Pajdla are with the Czech Technical University of Prague, Prague 121 35, Czech Republic (e-mail: ehlget1@cmp.felk.cvut.cz; pajdla@cmp.felk.cvut.cz).

D. Ammon is with the Daimler Group Research and Advanced Engineering, 89081 Ulm, Germany (e-mail: dieter.ammon@daimler.com).

Color versions of one or more of the figures in this paper are available online at <http://ieeexplore.ieee.org>.

Digital Object Identifier 10.1109/TITS.2008.2006815



Fig. 2. Catadioptric camera as a combination of lenses and mirrors. The black needle in the middle prevents internal reflections [3].

Geyer and Daniilidis [4] established a unifying theory for the six central catadioptric cameras. Due to its robustness and a small number of parameters, a similar model to this is used in the bird's eye view application, but with somewhat different interpretation of the parameters [5].

In [6], the theory and design of stereo catadioptric cameras are given. In this paper, however, the geometry of a pair of catadioptric cameras to obtain a technique for combining views is explored. As shown in [7], a stereo approach in automotive applications using catadioptric cameras is not robust enough. In contrast to [8], the baseline in our setup is too large to obtain reliable results in the vicinity of the vehicle. We will show how a robust vision system for automotive applications can be obtained where the driver is able to survey the whole surrounding area of his vehicle.

A. Omnidirectional Cameras in Automotive Applications

There are many systems integrated into modern automobiles that improve the safety and convenience of driving. These systems make use of different sensors to survey the vehicle surrounding. The data reach from nonvision sensors like radar or light detection and ranging (LIDAR) to vision sensors like night vision and backing up cameras.

A survey of vehicle surround capturing and obstacle detection using cameras is given in [9]. It stands out that none of the publications mentioned there deals with the problem of monitoring the surrounding area of trucks and trailers, where specific problems arise.

In [10], Gandhi and Trivedi presented a system that generates a 360° surround view map of an automobile. They introduced two different mounting positions of omnidirectional cameras. First, a single catadioptric camera was mounted above the roof of a car, capturing the surrounding area with a single camera. Since this setup is not suitable for series production, in the second setup, the cameras were mounted to the side mirrors. However, parts in front and behind the vehicle were not captured by the cameras and such not seen in the resulting map.

In [8], an omnidirectional stereo system consisting of two catadioptric cameras, which were mounted on the rear bumper

of a car, was described. A stereo algorithm [11] was applied to reconstruct the scene. The stereo system did not detect objects in the near surroundings of the sensors because the disparity in this area was very large. The reported error range increased to above 30 cm with obstacles 3 m away from the car. The main problem was the low and varying resolution in catadioptric images.

Gehrig [7] analyzed three different types of cameras for stereo vision in cars: conventional cameras mounted on a pan-tilt, catadioptric cameras, and fish-eye cameras. The cameras were placed on the left- and right-hand sides of the rear-view mirror. He concluded that the active stereo approach yielded the best result but had a limited field of view. The 3-D measurements obtained from catadioptric and fish-eye cameras are not very accurate but offer a complete field of view at any time. The fish-eye stereo setup uses a larger part of the imager than the omnidirectional cameras and yields better results.

To reduce the blind spot area in front of heavy goods vehicles, a stereo vision system consisting of two spherical lenses mounted below the windshield of the truck was introduced in [12]. An inverse perspective mapping (IPM) algorithm [13] back-projects every pixel of the camera and intersects the ray with the ground plane. This algorithm was applied to detect obstacles in front of the vehicle. If an obstacle was detected in front, the vehicle did not start. However, the cameras covered only the front area and not the whole surrounding area of the vehicle.

In the Protector project [14], a truck was equipped with three 24-GHz near-distance radar sensors mounted on the right-hand side. An acoustic as well as a visual warning was given to the driver if a bicyclist appeared on the right-hand side of the truck. However, as in [12], only parts of the surrounding area were covered by sensors.

In this paper, the positions of the cameras were optimized such that every point in the surrounding area is visible and the mounting positions were selected to be suitable for vehicle design and manufacturing.

We introduced the first bird's eye view systems for light and heavy commercial vehicles in [15] and [16]. In this paper, however, we present a detailed and complete description of a bird's eye view system that does not need any additional sensor instead of the cameras, which reduces the overall costs. Additionally, driving corridors that simplify the maneuvering of large vehicles are introduced. As far as we know, those corridors supporting the driver of heavy goods vehicle have not been shown before. The whole derivation of those corridors is presented, which is more complex than that for standard cars.

III. BIRD'S EYE VIEW

To obtain an intuitive view of the surroundings of a vehicle (Fig. 3), a virtual pinhole camera—the bird's eye—is placed above the vehicle. The bird's eye view algorithm generates the resulting image in two steps. First, for every pixel of the virtual pinhole camera, a ray is back-projected and intersected with the ground plane. Then, the intersection point with the ground plane is projected to one of the four catadioptric cameras mounted on the vehicle. The first step is similar to generating

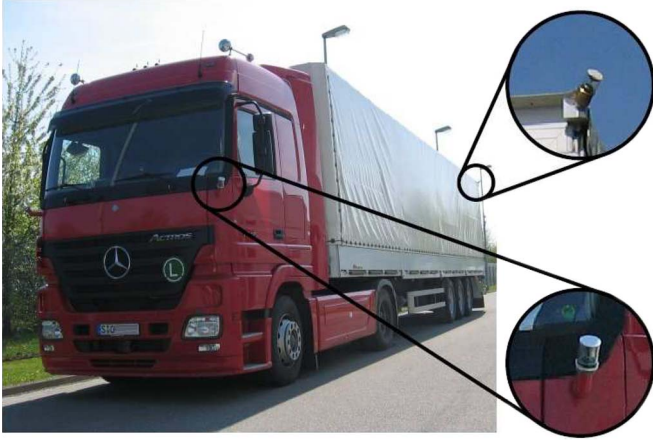


Fig. 3. Test vehicle equipped with four catadioptric cameras. Two were mounted on the truck and two on the trailer to cover the vehicle surroundings.

IPM images. However, instead of back-projecting the pixel of the actual cameras like in [13] and [17], the pixels of a virtual camera are back-projected, and the intersection with the ground plane is mapped to one of the four catadioptric cameras. The virtual camera simplifies the combination the four catadioptric camera images to a single bird's eye view image. In addition, the position of the virtual camera is changed according to the driving state to obtain an optimal image for different maneuvering situations. For instance, when the driver selects the reverse gear, the virtual camera is moved to the rear part of the vehicle.

This section provides a detailed description of the steps for generating a bird's eye view image. Since the back-projected rays of the virtual camera are intersected with the ground plane, the image is correct for objects on the ground plane. Objects that are not on the ground plane become distorted. This section shows how the bird's eye view image must be constructed to avoid disappearing of objects that are not located on the ground plane. In addition to that, driving corridors showing the path of motion of the vehicle are superimposed onto the resulting image. These corridors simplify the maneuvering of large vehicles.

A. Back Projection of Virtual Pinhole Pixels

Fig. 4 shows the virtual pinhole camera placed above the vehicle. A ray through the center C_p of this perspective camera and a pixel $\mathbf{X}_p = (x_p, y_p, f)$ in the pinhole coordinate frame is

$$g(\lambda) = C_p + \lambda(\mathbf{X}_p - C_p). \quad (1)$$

It is $C_p = (0, 0, 0)$ because C_p is the center of the pinhole coordinate frame

$$g(\lambda) = \lambda \mathbf{X}_p \quad (2)$$

hence $g(\lambda)$ represents a ray in pinhole coordinates.

Since we assume a flat world, the intersection \mathbf{X}_v of this ray with the ground plane $Y = 0$ yields

$$\mathbf{X}_v = \lambda \mathbf{R}_p \mathbf{X}_p + \mathbf{T}_p \quad (3)$$

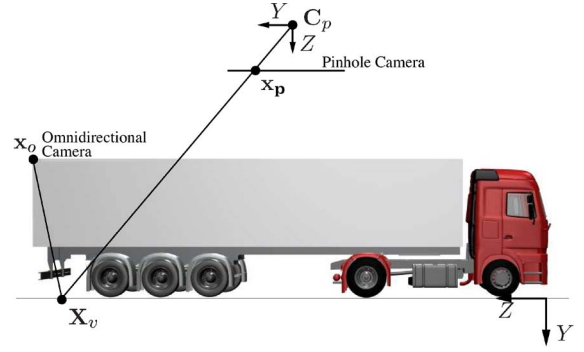


Fig. 4. Bird's eye view image is constructed in two steps. First, every pixel \mathbf{x}_p of the virtual pinhole camera—the bird's eye—is back-projected and intersected with the ground plane in the point \mathbf{X}_v . This point is projected to one of the four catadioptric cameras.

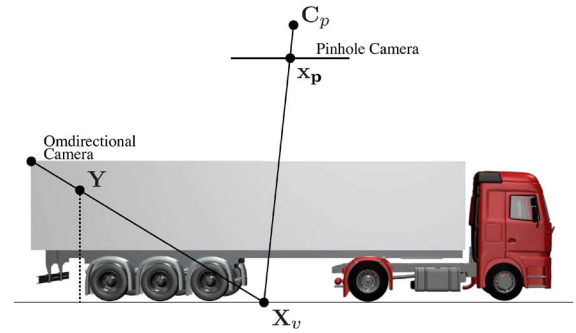


Fig. 5. Since the back-projected ray of the virtual pinhole camera is intersected with the ground plane, points located not on the ground plane are distorted. The point \mathbf{Y} not on the ground plane is seen in the resulting image at the pixel \mathbf{x}_p , which is the intersection of the ray through the point \mathbf{Y} and the center of the catadioptric camera with the ground plane.

where \mathbf{R}_p is the rotation matrix, and $\mathbf{T}_p = (t_x, t_y, t_z)^T$ is the translation vector of the pinhole camera. Since the Y coordinate of \mathbf{X}_v in vehicle frame must be zero at the intersection with the ground plane, λ can be determined as

$$\lambda = \frac{-t_y}{\mathbf{r}_2^T \mathbf{X}_p} \quad (4)$$

where \mathbf{r}_2 is the second row of the rotation matrix \mathbf{R}_p . Inserting λ into (2) results in the point \mathbf{X}_v on the ground plane that belongs to the pixel x_p .

Since the projection plane of the camera is parallel to the ground plane, the resulting image is a mere scaled version of the image on the ground. To efficiently compute the resulting bird's eye view image, a parallel projection is used. The pinhole projection is an intuitive way of selecting the areas of interests in the finale image. For instance, if the driver wants to turn right, the pinhole camera is moved to the left-hand side so that the driver is able to survey this area.

B. Selection of a Catadioptric Camera

Since the back-projected ray is intersected with the ground plane, points that are not located on the ground plane are distorted in the final image. As Fig. 5 illustrates, points not on the ground plane \mathbf{Y} are projected onto the ground plane at position \mathbf{X}_v and seen in the resulting image of the virtual

pinhole camera at pixel x_p . This must be kept in mind when the bird's eye view image is constructed from the four catadioptric cameras.

This section shows how to select a catadioptric camera such that the algorithm constructs a bird's eye view image that covers the whole surrounding area.

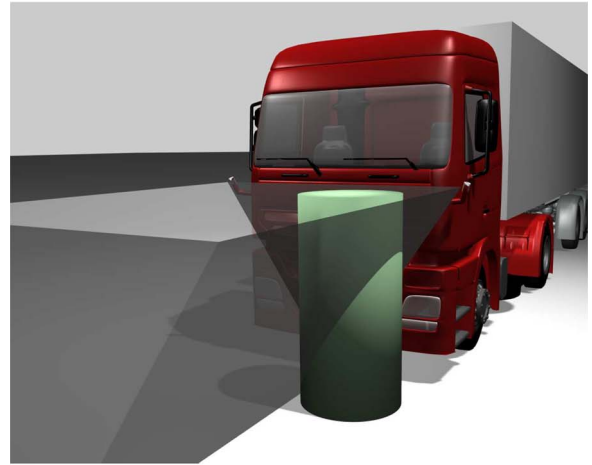
A naive approach to select a catadioptric camera for every point X_v on the ground plane is to choose the nearest camera to that point. This leads to a symmetric partitioning of the space. The left-hand side of the vehicle is covered by the front and rear cameras mounted on the driver's side of the vehicle, and the right-hand side is covered by the cameras mounted on the passenger's side. This results in stitching along the line of lateral symmetry of the vehicle in the resulting bird's eye view image. In this partitioning, every point on the ground plane is visible in the bird's eye view image. However, this is not true for points above the ground plane. Consider, for instance, a point with nonnegligible height placed in the middle of the truck. In the bird's eye view image of the left camera, it is mapped to a point on the ground plane that is on the right-hand side of the truck. However, this part is covered by the camera mounted on the passenger's side and is not seen in this camera. Thus, it is not seen in the resulting bird's eye view image. The same holds for the left-hand side, respectively.

Fig. 6(a) shows that points inside the blind wedge volume are not visible in the bird's eye view image when symmetric partitioning is chosen. The top of the cylinder is not visible in the resulting bird's eye view image because it will be projected to the passenger's side, and this one is covered by the camera mounted on the right-hand side. However, it is also not visible in the camera on the left-hand side because the cylinder is located on the driver's side. As the cylinder approaches the partitioning line, it will gradually become completely invisible in the resulting bird's eye view image.

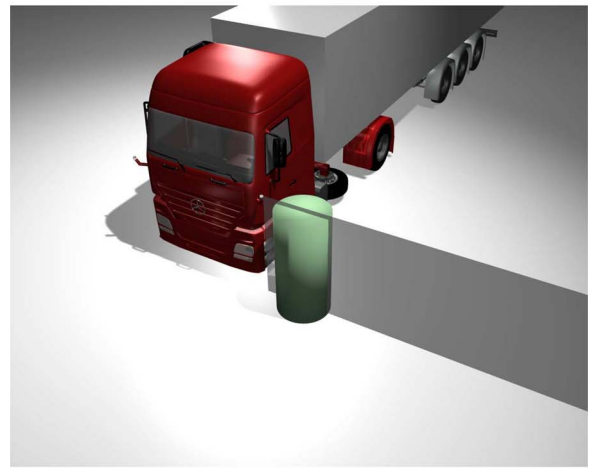
Such a blind wedge is avoided if an asymmetric partitioning along the baseline of the catadioptric cameras is used. As Fig. 6(b) shows, the asymmetric partitioning removes the blind volume. The rear part of the cylinder is visible in the camera mounted on the driver's side, and the front part is visible in the camera mounted on the passenger's side. As in the case of symmetric partitioning, both parts are projected to the ground plane, but in the same direction. Consequently, if an object moves across the partitioning plane, there is only a change in scale and no disappearing.

Fig. 7 shows two different situations where different partitioning approaches were applied to the same images. In Fig. 7(a) and (b), a person stands in front of the vehicle. Fig. 7(a) shows the resulting bird's eye view image if symmetric partitioning is used. The person is almost completely invisible. In Fig. 7(b), however, the person is well visible in the image. Fig. 7(c) and (d) shows a person standing at the partitioning plane of an asymmetric partitioning. The person is visible in both images. There is only a change of scaling when crossing the partitioning plane.

Fig. 8 illustrates the distortion caused by the flat world assumption. An object of 1-m height is placed at different positions around the vehicle; its distortion is described by the contour lines in the plot. The position of the separating plane



(a)



(b)

Fig. 6. (a) Blind wedge emerging in front of the truck when a symmetric partitioning is chosen. All points within the wedge are invisible in the bird's eye view image. The upper part of the cylinder is not visible in the resulting bird's eye view image because this part is projected to the area that is covered by the catadioptric camera at the right-hand side of the truck. As the cylinder approaches the middle of the vehicle, it gradually becomes invisible. (b) Partitioning along the baseline of the catadioptric cameras. If an object moves through the partitioning plane, only a change of scale of this object is visible in the resulting bird's eye view image, and there is no blind spot, and thus, everything is visible in the resulting image.

between truck and trailer is chosen such that the distortion is equal. This ensures a smooth transition from one camera to another.

It would also be possible to use only two catadioptric cameras mounted at the opposite corners of the vehicle. However, on one hand, the resolution of the cameras would be too low, and on the other hand, a blind wedge would emerge at the transition from one camera to the other so that a person standing in this transition would become invisible for the driver.

C. Projection to Catadioptric Camera

According to asymmetric partitioning, the point X_v is projected to one of the four catadioptric cameras. The cameras are calibrated w.r.t. a common coordinate system placed at the middle of the truck's front. The calibration can be done

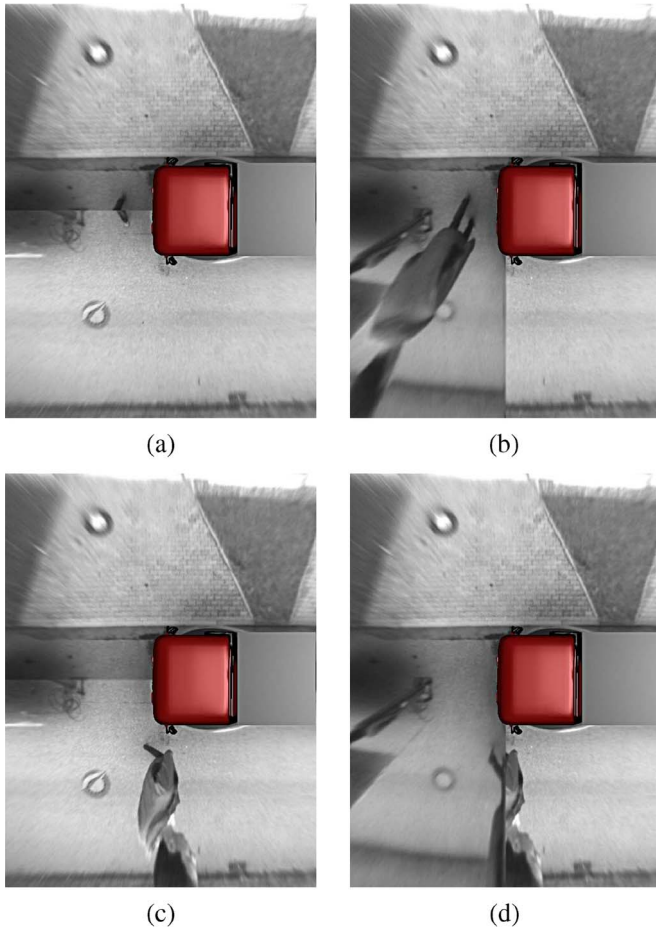


Fig. 7. (a) and (b) Same situation with different partitioning. The pedestrian standing in front of the truck is almost completely invisible when symmetric partitioning is applied. This is not true if asymmetric partitioning is used. (c) Pedestrian walking along the driver's side of the vehicle. The partitioning is symmetric. (d) Pedestrian crossing the partitioning plane of an asymmetric partitioning. The person is well visible while crossing the partitioning plane.

beforehand and kept fixed because the cameras are mounted in a fixed position. A detailed description of the calibration process can be found in [5]. Additionally, the kink angle between truck and trailer must be considered in this transformation. If the kink angle is not zero, the rotation with the center at the joint must be known to obtain correct bird's eye view image. The transformation consisting of a rotation R_k according to the kink angle and translation T_k to the joint is applied to the back-projected point X_v as

$$X_k = T_k^{-1} R_k T_k X_v. \quad (5)$$

Then, the point X_k is projected to one of the catadioptric cameras.

D. Driving Corridors

The previous sections showed how a bird's eye view image of the surrounding area is constructed. To support the driver in complicated maneuvering tasks, driving corridors are overlaid onto the bird's eye view image. These corridors show the path of the truck and trailer when the steering angle is kept constant.

Since the driving corridors are designed for maneuvering task with small velocities, a single-track model describing the path of motion of vehicles can be applied [18]. This model is extended to truck-trailer combinations, which result in direct calculation of the resulting kink angle when the vehicle moves. The single-track model assumes that two wheels of an axle can be considered as a virtual wheel placed in the middle of the axle. The axles are connected by rigid lines. Zero vehicle roll and a constant wheel load among the wheels are assumed. These assumptions are only valid for small velocities, which is the case while maneuvering.

Given an initial kink angle and a distance, the vehicle will move with constant steering angle, and the resulting kink angle can immediately be computed. A detailed description of the parameters and the derivation of the driving model is given in Appendix.

Fig. 9 shows four images of the resulting bird's eye view image with the overlaid corridors. Two corridors indicate the way the truck and trailer will move [Fig. 9(a)]. The corridors begin at the bumper of the truck and trailer, respectively, and end 5 m behind the vehicle. A line in the corridor is placed 1 m behind the truck and trailer, respectively.

The area that is covered by either the truck or trailer is marked in the bird's eye view image [Fig. 9(b)]. This marked region shows the areas that will be passed over by parts of the vehicle if the steering angle is kept constant.

The third corridor shows the position when the kink angle vanishes so that the truck and trailer are aligned straight. The distance that the vehicle has to travel until the kink angle vanishes is given by (20).

All three corridors assist drivers of large vehicles in complicated maneuvering tasks. The driver can place the corridors in the bird's eye view image to the position where truck and trailer should be placed after maneuvering by turning the steering wheel. Keeping the steering wheel fixed, the vehicle will move to this position.

IV. EVALUATION

The evaluation is divided into two parts. The first part discusses the resolution of catadioptric cameras. The second part deals with the model of the driving dynamics of the vehicle. We will show how accurately the single-track model approximates a real truck-trailer combination while maneuvering. A comparison between the calculated kink angle and the angle measured by a sensor placed at the joint of truck and trailer is made.

A. Resolution

The resolution of the bird's eye view image determines the area on the ground that is covered by a single pixel in one of the catadioptric cameras. Due to the large field of view of those cameras, the resolution must be considered since it may be the limiting factor of the performance. The resolution is examined in Fig. 10.

The figure shows a contour plot of a 2-D resolution function. This function shows the area covered by a back-projected pixel of the catadioptric camera as a function of the position on

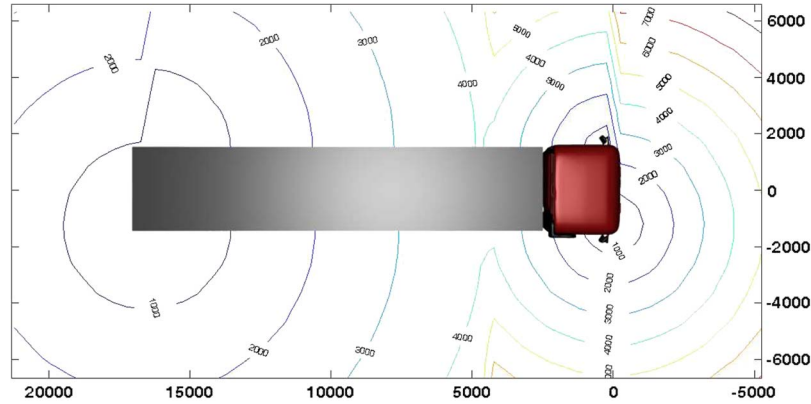


Fig. 8. Distortion caused by the flat world assumption. Since the cameras on the trailer are mounted higher, the distortion of these cameras is not as large as the one caused by the cameras mounted on the truck.

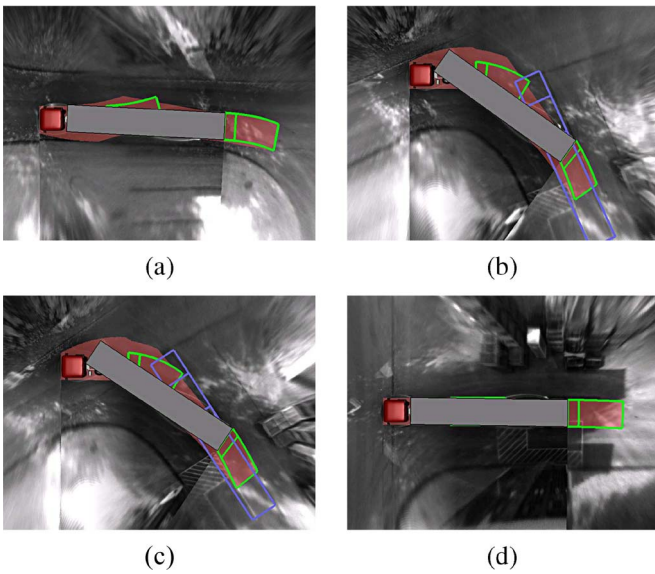


Fig. 9. (a) First and second corridor (green) begin at the bumper of the truck and trailer. They show the movement of the vehicle with the steering wheel kept fixed. (b) Third corridor (blue) showing the position where the kink angle vanishes so that the truck and trailer become aligned straight. The corridor can be placed in advance to the desired position by turning the steering wheel. (c) Area that is covered by the vehicle while driving is marked in the final bird's eye view image. (d) After placing the third corridor (blue) to the desired position, the steering angle is kept fixed, and the vehicle will end up parked to the position of this corridor.

the ground plane (the data are given in square millimeters). For instance, at the border of the front and rear cameras ($y = 5000$ mm), the area covered by a back-projected catadioptric camera pixel is 4000 and 16000 mm² for the front and rear cameras, respectively. That means two objects covering an area of 2000 mm² each (8000 mm² for the rear cameras) will be projected to the same pixel in the resulting bird's eye view image.

It can also be seen in Fig. 10 that the lowest sampling density is in the middle between the truck and the trailer. However, this area is well covered by the side mirrors mounted on the truck. The partitioning is selected in such a way that the lowest sampling area is either the area that is well covered by the side mirrors or in a region that is directly visible from the driver's position, like the partitioning in the front and rear parts of the vehicle.

B. Driving Corridors

This section compares the kink angle calculated by the single-track model as given by (18) with the measured kink angle given by a sensor mounted at the joint of the vehicle.

The measurement of the sensor [19] is based on an effect called the anisotropic magnetoresistive (AMR) effect. This effect causes a change of the resistance of the magnetic material that depends only on the direction of a magnetic field and not on the strength. Due to this effect, the sensor is very robust to shifts caused by thermal stress and to magnetic drift during lifetime. The sensor was placed at the shaft of the truck.

Fig. 11 shows the difference between the kink angle computation based on the model and the sensor. The solid curve indicates the sensor, whereas the dashed curve shows the curve calculated by the model given in (18). The sequence consists of 10000 frames that correspond to about 10-min driving. The inputs to the single-track model are steering angle and velocity. The maximum velocity was 23 km/h. The test run consisted of two 90° left turns (frame number 500 and 9000) and four 90° right turns (frame number 2000 to 8000). To achieve various kink angles, smaller sinusoidal turns were driven (frame number 750 to 2250 and 7750 to 9000). The maximum angle of left turns (positive angle) amount to 47.95° and was measured at frame number 9218. The maximum angle of right turns was 38.38°.

Fig. 12 shows four different driving situations using the computed kink angle. Fig. 12(a) corresponds to the first peak of Fig. 11 and conforms to the zenith of a left turn. Fig. 12(b) shows the situation after this turn was driven. This correlates to frame number 1000 in Fig. 11. The difference between the computed kink angle and the measured angle amounts to 1.16°. Fig. 12(c) shows the beginning of a turn. This conforms to frame number 7035. The difference is 1.27°. The largest difference 5.37° between the model and the sensors is shown in Fig. 12(d) and corresponds to frame number 9157. A slight misalignment of the front and rear bird's eye view image is visible.

V. CONCLUSION

The limited sight of drivers of heavy goods vehicle and buses can cause serious accidents. This paper has presented a system

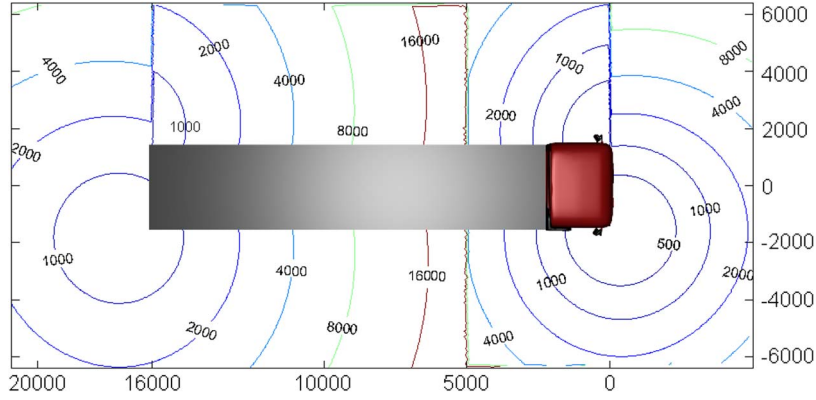


Fig. 10. Contour plot of a 2-D resolution function is shown. This function consists of x, y coordinates and shows the area covered by the back-projected pixel of the catadioptric cameras. All values are given in square millimeters.

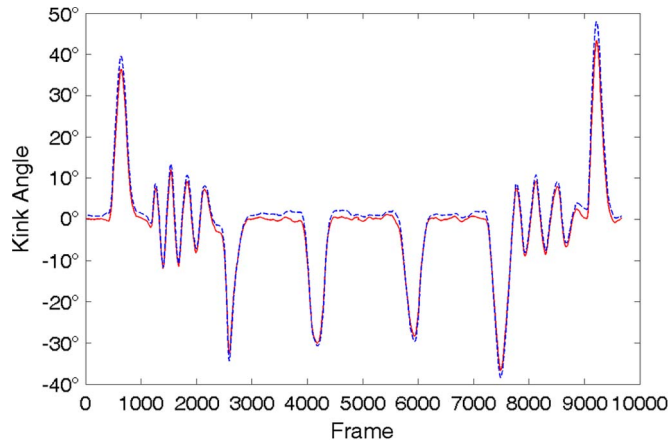


Fig. 11. Comparison between the kink angle determination based on the model introduced given by (18) and a sensor mounted on the joint of the vehicle. The dashed curve shows the kink angle of the sensor and the solid one the kink angle given by the single-track model introduced in Section I. The error mean amounts 0.0217, and the standard deviation is 0.0138, which shows that the model is very precise.

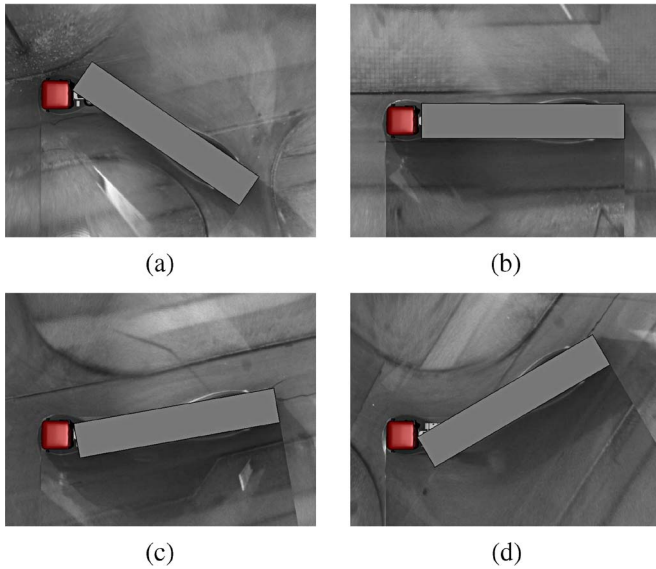


Fig. 12. (a) Frame number 645 in Fig. 11. The difference between the sensor and the model amounts to 3.07° . (b) Situation at frame number 1000, after the left turn was made. (c) Beginning of a right turn. (d) Bird's eye view image with the largest difference 5.37° between the model and the sensor. The driving corridors were switched off because the vehicle drove forward.

that combines the images of four cameras to obtain a view of the whole surrounding area of large vehicles and thus reduce accidents, and supports drivers on maneuvering tasks.

We have shown how the blind spot region looks like if the images are symmetrically stitched together, and that a stitching along the baseline of the cameras leads to a view without blind spots in the surrounding area. Such a system can be installed on any vehicle.

To correctly construct the bird's eye view image, the angle between truck and trailer must be known. This angle can be measured by a sensor mounted on the joint between truck and trailer. However, such a sensor can either not be installed or is too costly. By applying the presented single-track model, such a sensor is not necessary. Further, the single-track model can be used to overlay different driving corridors onto the resulting image, which simplifies the maneuvering of vehicles.

APPENDIX KINK ANGLE DETERMINATION

In Fig. 13, the steering angle at the front wheel is δ_r . This is the angle between the direction of travel v_v and the center line of the vehicle. The front wheel moves on a circle with radius r_f and has the curvature $\rho_f = 1/r_f$. The line orthogonal to the direction of motion of the front wheel and the line orthogonal to the center line at the second wheel of the truck intersect in P . The curvatures ρ_f and ρ_b can be computed from this triangle

$$\rho_f = \frac{\sin \delta_r}{l_{fb}} \quad (6)$$

$$\rho_b = \frac{\rho_f}{\cos \delta_r} \quad (7)$$

where l_{fb} is the distance from the front axle to the second axle of the truck.

The joint's path of motion is given by

$$\rho_c = \frac{\rho_b}{\sqrt{1 + (l_{bc}\rho_b)^2}} \quad (8)$$

where l_{bc} is the distance from the second axle to the joint. Compared to the center line, the path of motion of the joint

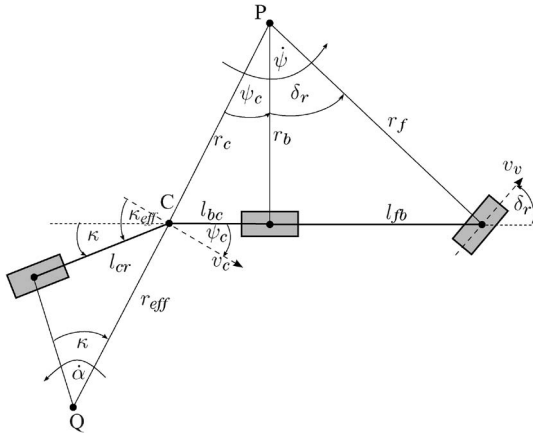


Fig. 13. Variables used to determine the motion path of the vehicle. The lengths l_{fb} , l_{bc} , and l_{cr} are measured in advance and kept fix. They describe the length from the front axle to the rear axle of the truck, from the rear axle to the joint, and from the joint to the rear axle of the trailer, respectively. The steering angle δ_r is measured by a sensor. The effective kink angle κ_{eff} is defined as the angle between the velocity vector of the joint and the trailer. The kink angle is the angle between the extension of the truck and trailer, and it is $\kappa_{\text{eff}} = \kappa + \psi_c$.

v_c is rotated by

$$\psi_c = \arctan l_{bc} \rho_b = \arcsin l_{bc} \rho_c. \quad (9)$$

The yaw rate of the truck is given by $\dot{\psi}$, and it depends on the velocity of the vehicle. It is

$$\dot{\psi} = v_v \rho_v = v_b \rho_b = v_c \rho_c \quad (10)$$

because we assume a single-track model without lateral acceleration.

The angle κ between the extension of the truck's center line and the center line of the trailer is the kink angle and is used in (5). The effective kink angle κ_{eff} is the angle between the path of motion of the joint and the trailer's center line. It is

$$\kappa = \kappa_{\text{eff}} + \psi_c. \quad (11)$$

To determine the change of the effective kink angle while driving, a differential approach must be applied. It is

$$r_{\text{eff}} = \frac{l_{cr}}{\sin \kappa_{\text{eff}}} \quad (12)$$

$$v_c = r_c \dot{\psi} = r_{\text{eff}} \dot{\alpha}. \quad (13)$$

Since ψ and α are the yaw angles of the truck and trailer, respectively, it is $\kappa_{\text{eff}} - \psi_c = \psi + \alpha$. This yields

$$\kappa_{\text{eff}}' = \dot{\psi} + \dot{\alpha} \quad (14)$$

because ψ_c is constant while driving.

Combining the last three equations and $r_c = (1/\rho_c)$ leads to

$$\kappa_{\text{eff}}'(\psi) = \frac{\sin \kappa_{\text{eff}}(\psi)}{l_{cr} \rho_c} - 1. \quad (15)$$

This differential equation determines the effective kink angle κ_{eff} after movement if the initial effective kink angle κ_0 , the steering angle δ_R , and the yaw rate $\sigma = l_t \cdot \rho_f$, where l_t is the

distance the vehicle will move with constant parameters, as well as the dimensions of the vehicle are known.

$$\text{Let } p := l_{cr} \rho_c \text{ and } q := \sqrt{|p^2 - 1|}$$

$$a(\kappa_0, \delta_R, \psi) := \exp\left(-\frac{q\psi}{p}\right) \frac{p \tan\left(\frac{\kappa_0}{2}\right) + 1 - q}{p \tan\left(\frac{\kappa_0}{2}\right) + 1 + q} \quad (16)$$

$$b(\kappa_0, \delta_R, \psi) := -\frac{q\psi}{2p} + \arctan\left(\frac{p \tan\left(\frac{\kappa_0}{2}\right) + 1}{q}\right). \quad (17)$$

Then, the kink angle κ_{eff} after the movement is

$$\kappa_{\text{eff}} = \begin{cases} 2 \arctan\left(\frac{q \frac{1+a(\kappa_0, \delta_R, \Psi)}{1-a(\kappa_0, \delta_R, \Psi)} - 1}{p}\right), & \text{if } |p| < 1 \\ 2 \arctan\left(\frac{q(b(\kappa_0, \delta_R, \Psi)) - 1}{p}\right), & \text{else} \end{cases} \quad (18)$$

If the steering angle vanishes, it is

$$\kappa_{\text{eff}} = 2 \arctan\left(\exp\left(\frac{l_t}{l_{cr}}\right) \frac{1 - \cos \kappa_0}{\sin \kappa_0}\right). \quad (19)$$

Thus, the effective kink angle κ_{eff} is given by these equations, and the kink angle of the trailer w.r.t. the truck is given by $\kappa = \kappa_{\text{eff}} - \psi_c$.

The distance l_{t0} , which the vehicle has to travel until the truck and trailer will be aligned straight, can be computed from (15) as

$$l_{t0} = \begin{cases} \frac{p}{\rho_f q} \log\left(\frac{(t_\kappa + \frac{q+1}{p})(t_\psi - \frac{q-1}{p})}{(t_\kappa - \frac{q-1}{p})(t_\psi + \frac{q+1}{p})}\right), & \text{if } |p| < 1 \\ \frac{2p}{\rho_f q} \left(\text{atan}\left(\frac{pt_\psi + 1}{q}\right) - \text{atan}\left(\frac{pt_\kappa + 1}{q}\right)\right), & \text{else} \end{cases} \quad (20)$$

where $t_k = \tan(\kappa_0/2)$, and $t_\Psi = \tan(\Psi_c/2)$.

REFERENCES

- [1] "Fitting blind-spot mirrors on existing trucks," *Consultation Paper*, Apr. 2006, Directorate-General For Energy And Transport.
- [2] S. Baker and S. Nayar, "A theory of single-viewpoint catadioptric image formation," *Int. J. Comput. Vis.*, vol. 35, no. 2, pp. 175–196, Nov./Dec. 1999.
- [3] H. Ishiguro, "Development of low-cost compact omnidirectional vision sensors," in *Panoramic Vision*. New York: Springer-Verlag, 2001, ch. 3, pp. 23–38.
- [4] C. Geyer and K. Daniilidis, "A unifying theory for central panoramic systems and practical implications," in *Proc. ECCV*, 2000, vol. 2, pp. 445–461.
- [5] C. Toepfer and T. Ehlgen, "A unifying omnidirectional camera model and its applications," in *Proc. Omnivis*, 2007, CD-ROM.
- [6] T. Svoboda and T. Pajdla, "Epipolar geometry for central catadioptric cameras," *Int. J. Comput. Vis.*, vol. 49, no. 1, pp. 23–37, Aug. 2002.
- [7] S. K. Gehrig, "Large-field-of-view stereo for automotive applications," in *Proc. Omnivis*, 2005, CD-ROM.
- [8] L. Matuszyk, A. Zelinsky, L. Nilsson, and M. Rilbe, "Stereo panoramic vision for monitoring vehicle blind-spots," in *Proc. IEEE Intell. Veh. Symp.*, Jun. 2004, pp. 31–36.
- [9] T. Gandhi and M. Trivedi, "Vehicle surround capture: Survey of techniques and a novel omni-video-based approach for dynamic panoramic surround maps," *IEEE Trans. Intell. Transp. Syst.*, vol. 7, no. 3, pp. 293–308, Sep. 2006.
- [10] T. Gandhi and M. M. Trivedi, "Motion based vehicle surround analysis using an omni-directional camera," in *Proc. IEEE Intell. Veh. Symp.*, Jun. 2004, pp. 560–565.
- [11] R. Labayrade, D. Aubert, and J.-P. Tarel, "Real time obstacle detection in stereovision on non flat road geometry through "v-disparity" representation," in *Proc. IEEE Intell. Veh. Symp.*, Jun. 2002, pp. 646–651.

- [12] M. Bertozzi, A. Broggi, P. Medici, P. P. Porta, and A. Sjogren, "Stereo vision-based start-inhibit for heavy goods vehicles," in *Proc. IEEE Intell. Veh. Symp.*, Jun. 2006, vol. 9, pp. 350–355. no. 1.
- [13] M. Bertozzi and A. Broggi, "GOLD: A parallel real-time stereo vision system for generic obstacle and lane detection," *IEEE Trans. Image Process.*, vol. 7, no. 1, pp. 62–81, Jan. 1998.
- [14] R. Cicilloni, "Protector final report," Commission Eur. Union, Brussels, Belgium, 1999. Tech. Rep..
- [15] T. Ehlgen and T. Pajdla, "Monitoring surrounding areas of truck-trailer combinations," in *Proc. Int. Conf. Comput. Vis. Syst.*, 2007. CD-ROM.
- [16] T. Ehlgen, M. Thom, and M. Glaser, "Omnidirectional cameras as backing-up aid," in *Proc. Omnivis*, Nov. 2007. CD-ROM.
- [17] H. A. Mallot, H. H. Bülthoff, J. Little, and S. Bohrer, "Inverse perspective mapping simplifies optical flow computation and obstacle detection," *Biol. Cybern.*, vol. 64, no. 3, pp. 177–185, Jan. 1991.
- [18] W. Schiehlen, Ed., *Dynamical Analysis of Vehicle Systems*. Udine, Italy: Springer-Verlag, 2008.
- [19] *KMA 200, Programmable Angle Sensor*, NXP, Eindhoven, The Netherlands.



Tobias Ehlgen received the Diploma in computer science from the University of Bonn, Bonn, Germany, in 2005. He is currently working toward the Ph.D. degree in electronic engineering and computer science with the Czech Technical University of Prague, Prague, Czech Republic.

From April 2005 to April 2008, he was with Daimler Research and Advanced Engineering Center, Ulm, Germany, where his work focused on the application of omnidirectional cameras in automotive environments. His research interests include

computer vision in the field of automotive environments.



Tomáš Pajdla received the M.Sc. and Ph.D. degrees from the Czech Technical University of Prague, Prague, Czech Republic.

He is currently with the Czech Technical University of Prague. He worked on the epipolar geometry of panoramic cameras, noncentral cameras, generalized epipolar geometries, structure from motion, minimal problems, and image matching. He participated in the development of vision-guided laser robotic welding, 3R measurement of hot steel rods, optical recognition of Braille prints, and tens of other

machine vision applications.

Dr. Pajdla is a member of the ACM and the Czech Pattern Recognition Society. His works were awarded prizes at OAGM 1998, BMVC 2002, and ICCV 2005.



Dieter Ammon received the Diploma in mechanical engineering and the Ph.D. degree from the Technical University of Karlsruhe, Karlsruhe, Germany, in 1985 and 1986, respectively.

Since 1986, he has been with the Daimler Group Research and Advanced Engineering, Ulm, Germany, where he developed advanced driving safety and comfort systems, as well as related analysis methods. He is currently a Senior Manager in the field of vehicle dynamics.